Research Square

Preprints are preliminary reports that have not undergone peer review.
They should not be considered conclusive, used to inform clinical practice,
or referenced by the media as validated information.

Catalytic Etherification of Furfuryl Alcohol to Isopropyl Furfuryl Ether over MIL-68(V) and MOF-Derived V_2O_3@C

Ubed SF Arrozi

ubedsonai.fmipa@um.ac.id

State University of Malang

Aryan B. Saputra

State University of Malang

M. Rafi Pratama

State University of Malang

Istifhamy Irnanda

State University of Malang

Surjani Wonorahardjo

State University of Malang

Yessi Permana

Institut Teknologi Bandung

Witri W. Lestari

Universitas Sebelas Maret

Wirawan Ciptonugroho

Universitas Sebelas Maret

Yudha P. Budiman

Universitas Padjadjaran

Khoa D. Nguyen

Ho Chi Minh City University of Technology (HCMUT), VNU- HCM

Hadi Nur

State University of Malang

Sheela Chandren

Universiti Teknologi Malaysia, UTM Johor Bahru

Lee H. Voon

Nanotechnology & Catalysis Research Centre (NANOCAT), Universiti Malaya

Research Article

Keywords: Etherification, furfuryl alcohol, isopropyl furfuryl ether, MIL-68(V), V2O3@C

Posted Date: September 2nd, 2026

DOI: https://doi.org/10.21203/rs.3.rs-10621097/v1

License: This work is licensed under a Creative Commons Attribution 4.0 International License.
Read Full License

Additional Declarations: No competing interests reported.

Abstract

A Vanadium-based metal–organic framework (MOF) and its carbon-supported oxide derivative (V_2O_3@C) were successfully prepared and evaluated as catalysts for the thermocatalytic etherification of furfuryl alcohol (FOL) with 2-propanol to produce isopropyl furfuryl ether (iPrFE). The parent material, MIL-68(V), exhibited superior catalytic performance, achieving complete FOL conversion with an iPrFE yield of 73% within 20 minutes at 160°C. By comparison, V_2O_3@C attained 74% FOL conversion after 3 hours under identical reaction conditions, delivering 66% iPrFE. Kinetic and thermodynamic investigations revealed that the reaction follows a pseudo-first-order kinetic model, with an apparent activation energy of 61 kJ mol^{-1}. In addition, the calculated $\Delta H^{\ddagger}$, $\Delta S^{\ddagger}$, and $\Delta G^{\ddagger}$ were 58 kJ·mol^{-1}, -154 J·mol^{-1}·K^{-1}, and 118 kJ·mol^{-1}, respectively. The heterogeneous nature of the catalyst was confirmed, demonstrating their potential for renewable iPrFE production.

INTRODUCTION

Chemical industries have increasingly shifted toward sustainable practices to produce high-quality chemicals from renewable resources. A key strategy in the transition is the utilization of biomass-derived compounds, particularly furan-based chemicals and their derivatives. Furan-derived compounds possess broad applicability across various sectors of the chemical industry. One representative example is furfuryl alcohol (FOL), which is produced through multistep conversion pathways from lignocellulosic biomass.[1–3] Subsequent reactions of FOL with alcohols enable its transformation into other valuable platform chemicals, including alkyl furfuryl ethers (AFEs) and alkyl levulinates (ALs).[4–8] Among these derivatives, AFEs have recently attracted considerable research interest. Due to their excellent thermal and chemical stability, high energy density, and elevated octane number, AFEs are considered promising candidates as biofuel components and fuel additives.[7,9,10]

Early studies reported that AFEs are generally synthesized from furfural (FAL) through direct reductive etherification[11,12] or dehydrative etherification of FOL[13,14] with aliphatic alcohols using homogeneous catalysts such as sulfuric acid (Fig. 1).[15] Previous studies on AFEs synthesis employed heterogeneous catalysts including clay minerals, zeolites, metals supported on carbon, sulphated materials, metal organic frameworks, and metal oxides.[6–8,16–29]

Yamanaka et al. reported the use of clay minerals montmorillonite K10 as heterogeneous catalysts for the dehydrative etherification of FOL. Despite achieving near-complete FOL conversion within 1 h, nitrogen pressures of up to 7 bar were still required.[26] In another study, Xu et al. examined a range of zirconium-modified zeolite for catalytic etherification of FOL with 2-propanol.[30] The catalyst favored the formation of isopropyl furfuryl ether (iPrFE), reaching selectivities of approximately 50%, although this was obtained using nearly stoichiometric catalyst amounts (~ 20 wt% relative to FOL). Moreover, the reaction system often relies on pressurized nitrogen gas. Efforts to use milder reaction conditions have been explored using alternative catalysts such as ZSM-5; but, these systems typically required catalyst

loadings of around 40 wt% relative to FOL.[24] Developing catalysts that can operate under milder conditions with reduced catalyst loadings while maintaining high activity and selectivity remains a critical challenge for practical implementation.

Metal–organic frameworks (MOFs) and their derived materials, including metal oxides dispersed within carbon matrices, have garnered significant interest due to their promising potential in gas separation and storage, as well as in heterogeneous catalysis.[31–34] MOFs are porous materials formed through coordination bonds between metal ions/ metal clusters and organic ligands. Their derived materials, produced through thermal or chemical conversion, preserve essential structural characteristics such as high surface area and intrinsic porosity, while offering improved thermal and chemical stability.[35–38] In comparison with conventionally synthesized metal oxides, these materials offer a greater density of uniformly accessible active sites, thereby enhancing catalytic efficiency. Moreover, their structural and compositional properties can be systematically tailored through the rational selection of precursors and templates.[39,40] Jin et al. reported that V_2O_3@C derived from vanadium-based MOFs functions as an effective catalyst for investigating the kinetics of polysulfide conversion in lithium–sulfur (Li–S) batteries.[41] In another study, Kim et al. prepared vanadium oxide- and carbide-based carbon composites via pyrolysis of MIL-47(V) and evaluated their catalytic performance in the liquid-phase oxidation of dibenzothiophene.[42]

Indeed, MOFs has been shown to actively catalyze etherification of furfuryl alcohol. Gupta et al. evaluated a sulfated Zirconium-based MOF, UiO-66(Hf)-SO_3H, as a catalyst for the etherification of furfuryl alcohol (FOL) with 2-propanol. Under reaction conditions of 120°C for 4 h, the catalyst achieved 77% FOL conversion, yielding 23% isopropyl furfuryl ether (iPrFE) and 52% isopropyl levulinate (iPrL).[43] Building on this work, Mulik et al. investigated the etherification of FOL with ethanol using a zirconium-based MOF, UiO-66–NH_2, as a support for phosphotungstic acid encapsulated within the MOF framework. This catalytic system demonstrated enhanced performance, reaching 97% FOL conversion after 4 h at 150°C.[44] Recently, our group demonstrated that the immobilization of $VOSO_4$ within a zirconium-based MOF, MOF-808, led to a remarkable enhancement in catalytic activity for the conversion of furfuryl alcohol into its corresponding furfuryl ethers and levulinates.[45]

In this study, Vanadium-based MOFs and its derivative (V_2O_3@C) were evaluated for the catalytic etherification of furfuryl alcohol (FOL) with 2-propanol. The reactions were conducted under thermocatalytic conditions using thermal heating. Catalyst loading, reaction time, temperature, and alcohol amount were systematically optimized. Reaction kinetics were further examined at three different temperatures to evaluate the temperature dependence of the reaction rate.

EXPERIMENTAL

Chemicals

The chemicals were used without further purification. Vanadium(IV) oxide sulfate hydrate ($VOSO_4 \cdot H_2O$, 97%), furfuryl alcohol (98%), 2-furfuraldehyde (≥98%), Terephthalic acid (98%), and tetrahydrofurfuryl alcohol (99%) were obtained from Shandong Hanjiang Chemical Co., Ltd. *N,N*-dimethylformamide (98%), formic acid (98%), ethanol (97%) and methanol (99%) were purchased from Smart-Lab. 2-propanol was obtained from Merck.

Characterization

Gas Chromatography equipped with a Flame Ionization Detector (GC-FID, PerkinElmer) was employed to analyze the reaction products. The instrument was fitted with a capillary column (30 m, DF = 0.25 µm, 0.32 mm i.d.) and an FID detector. The temperature program used was as follows: an initial oven temperature of 72 °C held for 2 min, followed by heating to 250 °C at a rate of 10 °C min^{-1}. The injector and detector temperatures were set to 250 °C and 275 °C, respectively. For qualitative product identification, an Agilent GC–MS system (8890–5977C) equipped with an Agilent 19091S-433 column was used, applying the same oven temperature profile as in the GC-FID measurement.

Powder X-ray diffraction (PXRD) measurements were conducted using a Rigaku Miniflex diffractometer with a Cu X-ray source. Fourier-transform infrared (FTIR) spectra were collected using a Bruker Alpha DRIFT system with KBr pellets. Surface area analysis based on the Brunauer–Emmett–Teller (BET) method was performed using a Tristar II Plus 3020 instrument. Morphological and elemental analyses were carried out using a FEI Inspect-S50 system equipped for Scanning Electron Microscopy with Energy-Dispersive X-ray spectroscopy (SEM–EDX).

Syntheses of Vanadium-based MOFs

The synthesis of MIL-68(V) was carried out via a solvothermal method adapted from the procedure reported by Barthelet et al. (2004).[46] In a typical preparation, 6 mmol of $VOSO_4 \cdot H_2O$ (0.978 g) and 6 mmol of terephthalic acid (0.997 g) were dissolved in dimethylformamide to a total solution volume of 100 mL. The solutions were sonicated until complete dissolution. Once homogeneous, the ligand solution was added to the metal precursor solution and stirred at room temperature for 30 min. The resulting mixture was transferred into a 100 mL Teflon-lined stainless-steel autoclave and heated at 180 °C for 20 h. The product was collected by centrifugation, followed by washing with ethanol 12 times over a period of three days. The obtained solid was then dried at 100 °C for 5 h.

Synthesis of V_2O_3@C

The V_2O_3@C catalyst was prepared via pyrolytic carbonization of MIL-68(V). In a typical procedure, approximately 0.3 g of MIL-68(V) was placed in a quartz boat and inserted into the tube of a tubular furnace under a continuous nitrogen flow. The furnace was heated to 600 °C at a rate of 10 °C min^{-1} and maintained at this temperature for 2 h. The resulting black powder was collected and stored in a desiccator.

Catalytic Test

Catalytic evaluations were carried out in a sealed system using a 10 mL Teflon-lined autoclave. In a typical experiment, 20 mg (0.0164 mmol) of catalyst—equivalent to 1% of the molar amount of furfuryl alcohol (FOL, 0.1470 g, 1.5 mmol)—and 2.5 mL (32.7 mmol) of 2-propanol were introduced into the reactor. The mixture was stirred at 600 rpm and allowed to react at the designated temperature and reaction time. Upon completion, the reaction mixture was filtered, and the filtrate was analyzed by GC-FID. To establish the optimum reaction conditions, a series of systematic variations were examined, including type of catalysts, catalyst loading, reaction temperature, and reaction time. Quantitative analysis of the reaction products were conducted using Gas Chromatography (GC). Due to the limited commercial availability of the reaction products, quantification was determined via the area normalization method. Qualitative identification and structural confirmation of the reaction components were established by Gas Chromatography-Mass Spectrometry (GC-MS)

Leaching tests were performed by conducting the reaction using 20 mg of catalyst, 1.5 mmol (0.147 g) of furfuryl alcohol (FOL), and 2.5 mL of 2-propanol at 160 °C. After the first 5 min, the reaction was stopped and the catalyst was separated from the filtrate by centrifugation. The filtrate was then analysed using GC-FID and was used for further reaction to observe any changes in the catalytic conversion over time. This catalytic result was compared with the same reaction but without catalyst separation.

The catalyst reusability was initiated by performing the reaction under the optimized reaction conditions. After the first reaction cycle, the spent catalyst was recovered and washed with ethanol 12 times over the course of three days, followed by drying in an oven at 100 °C for 5 h and activation under vacuum at 100 °C for 3 h. The reusability catalyst was then reused under identical reaction conditions. This sequence of use, recovery, washing, drying, and activation was repeated until two times.

The reaction kinetics were evaluated by performing experiments at three temperatures: 120 °C, 140 °C, and 160 °C. For each temperature, the reaction was carried out for 5, 10, and 15 min. The kinetic studies were conducted using 20 mg of catalyst, 1.5 mmol (0.147 g) of FOL, and 2.5 mL of 2-propanol in a 25 mL Teflon-lined autoclave.

RESULT AND DISCUSSION

Catalyst Synthesis

MIL-68(V) was synthesized *via* a solvothermal method by reacting $VOSO_4 \cdot H_2O$ with terephthalic acid (H_2BDC) in DMF as the solvent. Unlike zirconium MOFs, the use of a carboxylate modulator in the reaction mixture was avoided, as it lowers the reaction pH and retards the deprotonation rate of H_2BDC. This slower deprotonation facilitates structural reorganization toward the more compact and structurally complex MIL-88B(V) phase.[47] The corresponding carbon-supported metal oxide, V_2O_3@C, was prepared via pyrolysis of the MIL-68(V) precursor at 600 °C under a nitrogen atmosphere. This temperature was selected because vanadium-based MOFs are known to decompose at temperatures

above 500 °C.[48] The thermal treatment induced a distinct color change from green (MIL-68(V)) to black, indicating the formation of the carbonaceous composite material (Fig. S1).

The PXRD pattern of the synthesized MIL-68(V) is shown in Fig. 2a. The diffraction peaks are in good agreement with the simulated pattern (ICSD No. 222072), displaying characteristic reflections at 2θ = 4.9°, 8.3°, and 9.8°, which confirm the successful formation of a well-defined crystalline framework. In contrast, the PXRD pattern of V_2O_3@C indicates the presence of amorphous carbon along with a rhombohedral V_2O_3 phase (ICSD No. 064796). Distinct diffraction peaks at 2θ = 24.2°, 26.7°, 32.1°, and 40.7° are observed. No additional vanadium oxide phases are detected, suggesting that pyrolysis of MIL-68(V) under carbonization conditions effectively produces the V_2O_3@C composite.

The average crystallite sizes of MIL-68(V) and V_2O_3@C were calculated using the Debye–Scherrer equation derived from the PXRD patterns. The pyrolysis of MIL-68(V) to form V_2O_3@C increases structural defects, as evidenced by the reduced diffraction intensity and the broadening of peaks (higher full width at half maximum, FWHM). Thermal treatment to MIL-68(V) leads to a decrease in both crystallite size and overall crystallinity (73% to 69%). The calculated crystallite size of V_2O_3@C is 25.1 nm, which falls within the range typically reported for V_2O_3 (20–50 nm).[49]

MIL-68(V) and V_2O_3@C were characterized by FTIR to identify the functional groups present in the synthesized materials (Fig. 2b). The FTIR spectra of the MIL-68(V) show a shift in the absorption band from 1679 cm^{-1} in H_2BDC to 1688 cm^{-1} in MIL-68(V). This shift indicates that the C=O group of the carboxylate moiety in H_2BDC coordinated to the vanadium ions.[50] The FTIR spectra of V_2O_3@C reveals a prominent absorption band at 986 cm^{-1}, attributed to the symmetric stretching vibration of the V^{3+}=O bond. Additional bands at 875 cm^{-1} and 677 cm^{-1} are assigned to the stretching vibrations of V–O–V linkages, which are characteristic of vanadium oxide frameworks.[51] Moreover, the absorption peaks observed at 1272 cm^{-1} and 1618 cm^{-1} correspond to C–OH stretching and –OH bending vibrations, respectively, indicating the presence of residual hydroxyl groups on the material surface after thermal treatment.

The morphology of the synthesized materials was examined by SEM analysis. As illustrated in Fig. 2c, MIL-68(V) exhibits a well-defined hexagonal needle-like morphology. Upon pyrolysis, partial structural collapse occurs, resulting in the formation of amorphous domains, as shown in Fig. 3d. A significant decrease in particle size is observed following thermal treatment, from approximately 2700 nm for MIL-68(V) (Fig. 3e) to about 150 nm for V_2O_3@C (Fig. 3f). This particle size is consistent with the typical range reported for V_2O_3@C nanostructures (50–150 nm).[52]

The conversion of MIL-68(V) into its derived composite is governed by several factors, including the precursor structure, pyrolysis temperature, and reaction atmosphere. Under inert conditions, the organic linkers undergo in situ carbonization, forming porous carbon with a high specific surface area. Continued pyrolysis promotes the generation of vanadium oxide nanoparticles that are uniformly dispersed within

the carbon matrix, resulting in well-integrated metal oxide–carbon architectures that are challenging to obtain through conventional physical mixing approaches.[48]

Nitrogen physisorption measurements were conducted to determine the specific surface areas of the synthesized materials. The BET surface area of MIL-68(V) was found to be 91 $m^2 g^{-1}$, which is considerably lower than the values reported by Barthelet et al. (Table S1, Fig. S2).[46,50] This discrepancy may be attributed to the relatively lower crystallinity of the prepared vanadium MOFs. Furthermore, partial pore blockage by residual solvent molecules, uncoordinated organic linkers, metal species, and the presence of amorphous domains may further limit the accessible surface area.[53] Attempts to enhance crystallinity by adjusting reaction temperature and synthesis scale did not result in significant improvement. However, the V_2O_3@C composite, interestingly, exhibited a higher BET surface area (131 $m^2 g^{-1}$) than its parent MIL-68(V). This value is consistent with previous reports on carbon-supported vanadium oxide materials.[52]

Catalytic Study

The synthesized materials were then tested as catalysts in the catalytic etherification of FOL with 2-propanol. This was initially conducted by comparing the vanadium-MOF, V_2O_3@C and their precursors. Reactions were performed at 120 °C for 1 h using conventional heating in an oil bath. Control experiments, including a blank reaction (without catalyst) and a reaction catalyzed by terephthalic acid (H_2BDC), resulted in negligible FOL conversion (Table 1, entries 1 and 2). In contrast, the homogeneous catalyst of $VOSO_4 \cdot H_2O$ afforded 15% conversion of FOL producing 11% of iPrFE and 4% iPrL (Table 1, entry 3). The V_2O_3@C composite provided 12% FOL conversion with exclusive formation of iPrFE (Table 1, entry 5). Meanwhile, MIL-68(V) exhibited slightly higher FOL conversion (17%) but lower selectivity toward iPrFE (61%) and resulting in a comparable iPrFE yield of 10% (Table 1, entry 4). This suggests that the catalytic activity is attributed to the presence of vanadium species which act as Lewis acid sites. Moreover, the catalytic efficiency for the etherification of FOL varied significantly depending on the chemical environment and structure of the vanadium species. While MIL-68(V) shows slightly higher activity of V_2O_3@C, their product distributions revealed distinct differences in selectivity.

Table 1. The catalytic etherification reaction between furfuryl alcohol (FOL) and 2-propanol using various catalysts.[a]

Entry	Catalysts	Conversion of FOL (%)[b]	Yield (%)[b]		Selectivity to iPrFE (%)[b]
			iPrFE	iPrL	
1	Blank	0.3	0	0	0
2	H_2BDC	0	0	0	0
3	$VOSO_4{\cdot}H_2O$	15	11	4	75
4	MIL-68(V)	17	10	7	61
5	V_2O_3@C	12	12	0	100

[a] Reaction condition: 1.63 mmol FOL; (0.02 g/ 0.016 mmol) of catalyst; 2-propanol (2.5 mL; 32.7 mmol), T= 120 °C; t= 1 h.

[b] Calculated based on GC-FID.

The etherification of FOL with 2-propanol to form iPrFE proceeds via Lewis acid–catalyzed pathway. In both catalysts, the active Lewis acid sites are associated with V^{3+} ions, which interact with the hydroxyl group of FOL. Owing to the oxophilic nature of vanadium, this interaction facilitates –OH activation by shifting electron density toward the V^{3+} center, thereby increasing the electrophilicity of the adjacent carbon and promoting –OH elimination. This step leads to the formation of a carbocation intermediate, which is subsequently attacked by 2-propanol acting as a nucleophile to generate a protonated ether species. Deprotonation of this intermediate yields iPrFE, while the released proton temporarily binds to the catalyst surface.[54,55]

Reaction optimization was carried out to enhance the conversion of FOL over V_2O_3@C and MIL-68(V), with particular focus on the influence of reaction temperature. Temperature plays a decisive role in determining catalytic activity and product distribution. Accordingly, the etherification of furfuryl alcohol (FOL) with 2-propanol was performed at five different temperatures to assess its effect on catalytic performance. As summarized in Table 2, increasing the reaction temperature significantly improved FOL conversion for both catalysts. In the case of V_2O_3@C, raising the temperature from 80 to 160 °C led to a substantial increase in FOL conversion, from 13% to 74%. The iPrFE yield followed the same trend, increasing from 13% to 66%. A similar enhancement in FOL conversion with increasing temperature was observed for MIL-68(V), rising from 42% at 80 °C to 99% at 100 °C. However, further temperature increases resulted in a pronounced decline in selectivity toward iPrFE, decreasing sharply from 75% at 80 °C to only 7% at 160 °C. This loss of selectivity is attributed to the formation of isopropyl levulinate (iPrL), produced via thermal ring-opening of iPrFE at elevated temperatures, thereby reducing the proportion of the desired ether product. Overall, these findings underscore the critical influence of reaction temperature on catalytic activity and product selectivity in the etherification process. This behavior is in agreement with the findings reported by Gupta et al. and Hu et al., who showed that higher reaction

temperatures promote secondary reactions, thereby reducing selectivity toward iPrFE.[19,21,29] In Addition, an inverse relationship was observed between textural properties and reactivity; although V_2O_3@C possesses a a higher BET surface area, the parent MIL-68(V) proved more kinetically active. This higher conversion rate, however, came at the expense of iPrFE selectivity.

Table 2. Transformation of furfuryl alcohol (FOL) using various temperatures.[a]

Entry	Catalysts	T (°C)	Conversion of FOL (%)[b]	Yield (%)[b]		Selectivity to iPrFE (%)[b]
				iPrFE	iPrL	
1	MIL-68 (V)	80	42	31	11	75
2	MIL-68 (V)	100	99	57	32	57
3	MIL-68 (V)	120	100	61	35	61
4	MIL-68 (V)	140	100	60	36	60
5	MIL-68 (V)	160	100	7	93	7
6	V_2O_3@C	80	13	13	0	100
7	V_2O_3@C	100	13	13	0	100
8	V_2O_3@C	120	19	19	0	100
9	V_2O_3@C	140	20	20	0	100
10	V_2O_3@C	160	74	66	8	89

[a]Reaction condition: 1.63 mmol FOL; 0.02 g of catalyst; 2-propanol (2.5 mL; 32.7 mmol), t= 3 h.

[b]Calculated based on GC-FID.

Reaction time was also found to strongly influence the catalytic performance of the catalysts. As shown in Fig. 4a, FOL conversion at 160 °C increased progressively with reaction time, rising from 13% at 5 min to over 70% after 180 min. The iPrFE yield increased rapidly during the initial stage, exceeding 25% within 30 min, and continued to improve at longer durations. The highest performance was achieved at 180 min, affording 74% conversion, 66% iPrFE yield, and 89% selectivity. Meanwhile, in the presence of MIL-68(V), the FOL conversion reached 44.8% within the first 5 min, accompanied by an iPrFE yield of 36%. The conversion increased progressively and attained complete conversion after 15 min, at which point the iPrFE yield increased to 62%. The maximum iPrFE yield (65%) was obtained at 20 min. Prolonging the reaction time beyond this point resulted in a gradual decline in iPrFE yield, accompanied by the increased formation of iPrL, which continued to accumulate up to 180 min. This trend indicates that extended reaction durations favor secondary reactions, whereby the initially formed iPrFE undergoes further

transformation into downstream derivative products. Among the examined conditions, the reaction performed at 160 °C for 180 min delivered the highest FOL conversion and iPrFE yield over V_2O_3@C, whereas MIL-68(V) achieved comparable performance within only 20 min at the same temperature. The markedly steeper reaction profile observed under these conditions indicates a higher etherification rate, corresponding to rapid FOL consumption and efficient iPrFE formation. Accordingly, these conditions were selected as optimal and were employed for subsequent optimization studies based on the observed reaction trends.

Because substrate concentration can significantly influence reaction kinetics, catalyst–substrate interactions, and overall product yield, the effect of FOL concentration was investigated to determine the optimal substrate loading for the etherification reaction. As shown in Table 3 (entries 1–3), increasing the FOL loading led to a pronounced decrease in conversion. Specifically, FOL amounts of 1.5, 2.0, and 2.5 mmol resulted in conversion values of 100%, 84%, and 77%, respectively. At a fixed catalyst loading and reaction time, higher substrate concentrations lead to a larger proportion of unreacted FOL, thereby lowering the overall conversion. This behavior can be attributed to the limited number of accessible active sites relative to the increased amount of substrate. Consequently, longer reaction times are required to achieve complete conversion when higher FOL loadings are employed.[56] Similarly, although increasing the amount of 2-propanol initially leads to a slight increase in FOL conversion (Table 3, entries 6 and 7), an excessive amount of 2-propanol results in a decline in FOL conversion (Table 3, entries 5 and 8). This suggests that an optimal alcohol concentration is required to balance substrate–catalyst interactions and maintain efficient catalytic performance.

Table 3. Optimization of etherification of furfuryl alcohol (FOL) and 2-propanol.[a]

Entry	Cat.	FOL conc. (mmol)	Vol. of 2-propanol (mL)	Conv. (%)[b]	Yield (%)[b]		Selectivity to iPrFE (%)[b]
					iPrFE	iPrL	
1	MIL-68 (V)[c]	1.63	2.5	100	65	27	65
2	MIL-68 (V)[c]	2	2.5	84	55	22	73
3	MIL-68 (V)[c]	2.5	2.5	77	45	25	73
4	MIL-68 (V)[c]	1.63	2	100	73	24	73
5	MIL-68 (V)[c]	1.63	3	77	63	23	63
6	V_2O_3@C[d]	1.63	2	66	60	6	91
7	V_2O_3@C[d]	1.63	2.5	74	66	8	89
8	V_2O_3@C[d]	1.63	3	66	59	7	89

[a] Reaction condition: 0.02 g of catalyst; T= 160 °C.

[b] Calculated based on GC-FID.

[c] t = 20 min

[d] t = 180 min

The effect of catalyst dosage on FOL conversion and iPrFE yield was investigated for both V_2O_3@C and MIL-68(V) catalysts. As shown in Fig. 4b, the reaction catalyzed by 0.02 g of V_2O_3@C exhibited the best performance, achieving 74% FOL conversion and 66% iPrFE yield. Increasing the catalyst loading to 0.04 g resulted in a decrease in both conversion and yield, suggesting that excessive catalyst amounts negatively affect reaction efficiency. The optimal catalyst loading corresponds to approximately 13 wt% relative to the substrate, which is significantly lower than previously reported values (up to 40 wt%). [24] In contrast, varying the catalyst loading for MIL-68(V) did not lead to a significant improvement in either FOL conversion or product selectivity. Therefore, 0.015 g (≈10 wt% relative to FOL) was identified as the optimal catalyst dosage for the reaction. Notably, this value is also considerably lower than those reported in earlier studies. [24]

Reaction time and catalyst loading exert similar influences on the etherification of FOL to iPrFE. Increasing both parameters initially promotes the formation of iPrFE due to the greater availability of

active sites and longer contact time between the reactants and catalyst. However, at higher catalyst loadings or prolonged reaction times, the yield of iPrFE declines as a result of the formation of isopropyl levulinate (iPrL) as a side product.[21] This observation is consistent with previous studies indicating that iPrFE can undergo further conversion into iPrL under more severe reaction conditions, highlighting the importance of carefully controlling these parameters to maintain high selectivity. Mechanistically, the reaction proceeds through the nucleophilic substitution of FOL by 2-propanol to form iPrFE, accompanied by partial conversion to iPrL, in agreement with literature reports.[55] Mechanistically, the reaction proceeds through the nucleophilic substitution of FOL by 2-propanol to form iPrFE, accompanied by partial conversion to iPrL, in agreement with literature reports.[55]

Table 4. Comparative evaluation of the current catalytic system with literature-reported catalysts.

No	Catalysts	Alcohols	T (°C)	t (h)	P (bar)[a]	Conv (%)	%Yield AFEs	%Yield ALs	Ref.
1	ZSM-5[b]	Ethanol	40	3	-	9	7	-	[24]
2	Montmorillonite K10	Ethanol	140	1	8 (N_2)	>99	30	26	[26]
3	Zr/CZ[c]	2-Propanol	180	1	10 (N_2)	99	40	>80	[30]
4	Zr/NPZ[c]	2-Propanol	180	1	10 (N_2)	100	30	>70	[30]
5	Zr@NPZ[c]	2-Propanol	180	1	10 (N_2)	100	30	>80	[30]
6	SiO_2–Al_2O_3	2-Propanol	220	6	-	100	59	26	[22]
7	UiO-66(Zr)-SO_3H	2-Propanol	120	4	-	77	23	52	[29]
8	UiO-66(Hf)-SO_3H	2-Propanol	120	4	-	100	-	88	[29]
9	$VOSO_4$@MOF 808[d]	2-Propanol	150	5	-	94	64	25	[17]
10	MIL-68(V)[e]	2-Propanol	160	0,3	-	100	73	24	This work
11	V_2O_3@C[e]	2-Propanol	160	3	-	74	66	8	This work

[a] External Pressure, [b] Catalyst = 40 wt%, [c] Catalyst = 20 wt%, [d] Catalyst = 12 wt%, [d] Catalyst = 10-13 wt%

Under relatively mild conditions, the V_2O_3@C catalyst demonstrated good catalytic performance using 13 wt% of catalyst at 160 °C for 3 h. In contrast, complete FOL conversion and an iPrFE yield of 72.6% was achieved over MIL-68(V) using only 10% of catalyst at 160 °C for 20 min, indicating its superior catalytic efficiency. In comparison, Zr/Hβ and Sap-Zr catalysts require harsher reaction conditions and still afford iPrFE yields below 50%.[57,58] Both V_2O_3@C and MIL-68(V) exhibit clear advantages in terms of activity and selectivity. In addition, Table 4 compares the catalytic performance of the present system with previously reported catalysts for the etherification of FOL with aliphatic alcohols. Among the systems surveyed, MIL-68(V) and V_2O_3@C display superior activity. Importantly, the reaction proceeds slightly under atmospheric pressure with a relatively low catalyst loading of 10-13 wt%, whereas many literature-reported systems require higher catalyst dosages and/or elevated pressure.

Reaction Kinetics

To better elucidate the reaction kinetics, an investigation was carried out by tracking the temporal evolution of FOL concentration under controlled reaction conditions. The reaction order was determined by monitoring the change in FOL concentration as a function of time. Reaction kinetics were evaluated by plotting 1/[FOL] versus time for a second-order model and $\ln([C]_0 - [C])$ versus time for a pseudo-first-order model. As shown in Fig. 5a, the reaction is more likely to follow a pseudo-first-order kinetics. Although the reaction involves more than one reactant, the results suggest that the reaction rate is predominantly governed by the concentration of FOL. The observed rate constants (k_{obs}) are found to increase with the increase of reaction temperature, consistent with the Arrhenius relationship, where higher temperatures enhance reaction rates by increasing the kinetic energy of reacting species, enabling them to overcome the activation energy barrier. In the pseudo-first-order kinetic equation, k_{obs} represents the apparent rate constant, where an increase in k_{obs} reflects an enhancement in reaction kinetics.

The effect of temperature on the reaction rate was further evaluated using the Arrhenius equation, which provides insight into the activation energy (E_a) associated with the reaction. A plot of $\ln k_{obs}$ versus 1/T (Fig. 5c) yields a slope with a value of 61 kJ mol^{-1}. This value indicates that the reaction proceeds with relatively low energy. The thermodynamic parameters of the reaction, including $\Delta H^{\ddagger}$ and $\Delta S^{\ddagger}$, were calculated by using the Eyring equation. By plotting the values of $\ln(k_{obs}/T)$ against 1/T (Fig. 5d), The calculated values of $\Delta H^{\ddagger}$, $\Delta S^{\ddagger}$, and $\Delta G^{\ddagger}$ were 58 kJ·mol^{-1}, −154 J·mol^{-1}·K^{-1}, and 118 kJ· mol^{-1}, respectively. The positive $\Delta H^{\ddagger}$ indicates that formation of the transition state requires heat input to break bonds in the reactants, confirming the endothermic nature of the FOL etherification reaction. The negative $\Delta S^{\ddagger}$ suggests a decrease in entropy during the transition state formation, reflecting a more ordered system arising from the close interaction between the alcohol and substrate at the catalyst active sites. The positive $\Delta G^{\ddagger}$ indicates that the reaction is non-spontaneous and requires thermal energy to proceed and reach the transition state.

Leaching and Reusability Tests

Leaching tests were conducted to evaluate the heterogeneous nature of the catalyst under liquid-phase reaction conditions. Within the first 5 min, a conversion of 44.8% FOL was observed (Fig. 4c). After catalyst removal, the conversion increased only slightly to 45.6% and 45.8% at 10 and 15 min, respectively. In contrast, reactions performed without catalyst separation reached conversions of 73.9% and 100% at the same time intervals. The pronounced difference in conversion clearly indicates the absence of leached active species after catalyst removal, confirming the heterogeneous character of MIL-68(V).

Catalyst reusability was evaluated by reusing MIL-68(V) for two consecutive cycles (Fig 4d). The fresh catalyst achieved complete conversion in the initial run. Prior to reuse, the catalyst was extensively washed with 70% ethanol, dried at 100 °C, and reactivated under vacuum at the same temperature. However, the first and second reuse cycles showed a significant decline in conversion to 31% and 21.7%, respectively. This deactivation might be attributed to structural degradation of MIL-68(V), as evidenced by the disappearance of the diffraction peak at 2θ = 4.8°, reduced intensity at 2θ = 9.6°, and increased amorphous character (Fig S3).

CONCLUSION

Comprehensive characterization using PXRD, FTIR, SEM, and nitrogen physisorption confirmed the successful synthesis of MIL-68(V). Pyrolysis of MIL-68(V) produced V_2O_3@C with well-defined crystalline V_2O_3 phases and preserved textural properties, as evidenced by PXRD and physisorption analyses. The catalytic performance of all materials was evaluated for the etherification of furfuryl alcohol with 2-propanol to produce isopropyl furfuryl ether (iPrFE), with isopropyl levulinate (iPrL) formed as a side product. Among the catalysts investigated, MIL-68(V) exhibited the highest activity, achieving a complete conversion of FOL with an iPrFE yield of 73% and a side-product iPrL yield of 24% within 20 min at 160°C. In comparison, V_2O_3@C only afforded 74% of FOL conversion after 3 h at the same reaction temperature, yielding 66% iPrFE with only 8% iPrL as the side product. Kinetic and thermodynamic analyses indicated that the etherification reaction follows a pseudo-first-order kinetic model, with an activation energy of 61 kJ mol^{-1}. The calculated activation parameters ($\Delta H^{\ddagger}$ = 58 $kJ{\cdot}mol^{-1}$, $\Delta S^{\ddagger}$ = −154 $J{\cdot}mol^{-1}{\cdot}K^{-1}$, and $\Delta G^{\ddagger}$ = 118 $kJ{\cdot}mol^{-1}$) indicate an endothermic and kinetically controlled process. Leaching tests confirmed the heterogeneous nature and structural stability of the catalyst, although a gradual decline in catalytic activity was observed during subsequent reuse cycles.

Declarations

Ethical Approval

Not applicable

Competing interests

The authors declare no competing interests

Authors' contributions

M. R. Pratama, A. B. Saputra, and I. Irnanda: Initial manuscript writing, Investigation, Formal Analysis, Visualization; Yessi Permana: Resources, Review & Editing; W. W. Lestari, W. Ciptonugroho, Y. P. Budiman, K. D. Nguyen, S. Chandren, L. H. Voon: Funding Acquisition, Project Administration, Review & Editing. S. Wonorahardjo, H. Nur: Supervision, review & Editing, Ubed SF Arrozi: Conceptualization, Methodology, Investigation, Validation, Supervision, Manuscript writing, Review & Editing, Resources, Funding Acquisition, and Project Administration.

Availability of data and materials

The data presented in this article will be available on request from the corresponding author

ACKNOWLEDGMENT

This project was supported by The State University of Malang under Contract Nos. 14.4.74/UN32.14.1/LT/2025 (Scheme: Indonesia Research Collaboration) and 24.2.445/UN32.14.1/LT/2025 (Scheme: Shining Star).

References

1. B. Y. Karlinskii, V. P. Ananikov, “Recent advances in the development of green furan ring-containing polymeric materials based on renewable plant biomass” *Chem Soc Rev* **2023**, *52*, 836–862.
2. J. Long, W. Zhao, H. Li, S. Yang, “Chapter 11 - Furfural as a renewable chemical platform for furfuryl alcohol production” *Biomass, Biofuels, Biochemicals: Recent Advances in Development of Platform Chemicals* **2020**, 299–322.
3. S. Zhang, Y. C. He, C. Ma, “Transformation of D-xylose into furfuryl alcohol via an efficient chemobiological approach in a benign deep eutectic solvent lactic acid:betaine-water reaction system” *J Mol Liq* **2024**, *410*, 125576.
4. Y. B. Huang, T. Yang, M. C. Zhou, Y. F. H. Pan, “Microwave-assisted alcoholysis of furfural alcohol into alkyl levulinates catalyzed by metal salts” *Green Chemistry* **2016**, *18*, 1516–1523.
5. D. Zhao, P. Prinsen, Y. Wang, W. Ouyang, F. Delbecq, C. Len, R. Luque., “Continuous Flow Alcoholysis of Furfuryl Alcohol to Alkyl Levulinates Using Zeolites” *ACS Sustainable Chemistry & Engineering* **2018**, *6*, 6901–6909.
6. A. L. Nuzhdin, Y. Wang, E. N. Vlasova, M. V. Bukhtiyarova, I. G. Danilova, S. A. Yashnik, A. A. Pochtar, L. Xiao, W. Wu, G. A. Bukhtiyarova, “Continuous-flow reductive etherification of furfural over CuAlO catalyst combined with HZSM-5-Al_2O_3 composite” *Fuel* **2024**, *356*, 129622.
7. Y. Wang, Q. Cui, Y. Guan, P. Wu, “Facile synthesis of furfuryl ethyl ether in high yield via the reductive etherification of furfural in ethanol over Pd/C under mild conditions” *Green Chemistry* **2018**, *20*,

2110–2117.

8. A. Hassine, A. I. Ayad, A. O. Dris, D. Luart, E. Guénin, “Continuous Flow Synthesis of Furfuryl Ethers over Pd/C Catalysts via Reductive Etherification of Furfural in Ethanol” *Catalysts* **2024**, *14*, 617.
9. K. Yang, R. Wang, D. Xu, X. Ma, D. Ding, M. Zhang, L. Zhang, Z. Bai, Z. Zhu, H. Lü, “Metal-acid dual sites in Pd/SiO_2-Al_2O_3 synergistically catalyze selective hydrogenation-etherification of furfural to bioether” *Catalysis* **2023**, *425*, 170–180.
10. M. Song, C. Qiu, P. Ma, J. Zhong, Z. Zhang, W. Fang, W. Song, J. Fan, W. Lai, “Effect of Lewis and Brønsted acidity in Ni/ZSM-5 on catalytic reductive etherification of furfural and alcohols” *Renewable Energy* **2023**, *212*, 468–477.
11. T. A. Natsir, S. Shimazu, “Fuels and fuel additives from furfural derivatives via etherification and formation of methylfurans” *Fuel Process Technol* **2020**, *200*, 106308.
12. C. Lluna-Galán, L. Izquierdo-Aranda, Dr. R. Adam, Dr. J. R. Cabrero-Antonino, “Catalytic Reductive Alcohol Etherifications with Carbonyl-Based Compounds or CO_2 and Related Transformations for the Synthesis of Ether Derivatives” *ChemSusChem* **2021**, *14*, 3744–3784.
13. J.-P. Lange, E. van der Heide, J. van Buijtenen, R. Price, “Furfural—A Promising Platform for Lignocellulosic Biofuels” *ChemSusChem* **2012**, *5*, 150–166.
14. J. R. Haan, J.-P. Lange, *Gasoline Composition And Process For The Preparation Of Alkylfurfuryl Ether*, **2009**, WO/2009/077606.
15. J.-P. Lange, “Furfural manufacture and valorization – A selection of recent developments” *Catalysis Today* **2024**, *435*, 114726.
16. D. Padovan, A. Al-Nayili, C. Hammond, “Bifunctional Lewis and Brønsted acidic zeolites permit the continuous production of bio-renewable furanic ethers” *Green Chemistry* **2017**, *19*, 2846–2854.
17. U. S. F. Arrozi, I. Irnanda, M. R. Pratama, Y. Permana, S. H. Qurbayni, W. W. Lestari, W. Ciptonugroho, H. W. Wijaya, Y. P. Budiman, “Etherification of furfuryl alcohol catalyzed by vanadium-modified MOF-808: Thermocatalysis and UV-assisted thermocatalysis” *Applied Catalysis A: General* **2025**, *706*, 120472.
18. M. Paniagua, J. A. Melero, J. Iglesias, G. Morales, B. Hernández, C. López-Aguado, “Catalytic upgrading of furfuryl alcohol to bio-products: Catalysts screening and kinetic analysis Author links open overlay panel” *Applied Catalysis A: General* **2017**, *537*, 74–82.
19. M. M. Antunes, S. Lima, P. Neves, A. L. Magalhães, E. Fazio, A. Fernandes, F. Neri, C. M. Silva, S. M. Rocha, M. F. Ribeiro, M. Pillinger, A. Urakawa, A. A. Valente, “One-pot conversion of furfural to useful bio-products in the presence of a Sn,Al-containing zeolite beta catalyst prepared via post-synthesis routes” *Journal of Catalysis* **2015**, *329*, 522–537.
20. T. A. Natsir, T. Hara, N. Ichikuni, S. Shimazu, “Kaolinite Catalyst for the Production of a Biodiesel-Based Compound from Biomass-Derived Furfuryl Alcohol” *ACS Applied Energy Materials* **2018**, *1*, 2460–2463.
21. L. Hu, B. Sha, Y. Shi, N. Shen, M. Yang, K. Chen, Z. Wu, X. Tang, A. He, L. Lin, “Switchable transformation of biomass-derived furfural to furfuryl alcohol and isopropyl furfuryl ether over a

zirconium-based bifunctional catalyst" *Chemical Engineering* **2024**, *498*, 155725.

22. Q. Cao, W. Zhang, S. Luo, R. Guo, D. Xu, "Synthesis of Furanic Ethers from Furfuryl Alcohol for Biofuel Production" *Energy & Fuels* **2021**, *35*, 12725–12733.
23. S. Chung, S. de Haart, R. Parton, N. Raveendran Shiju, "Conversion of furfuryl alcohol into alkyl–levulinates using solid acid catalysts" *Sustainable Chemistry for Climate Action* **2022**, *1*, 100004.
24. D. R. Chaffey, T. E. Davies, S. H. Taylor, A. E. Graham, "Etherification Reactions of Furfuryl Alcohol in the Presence of Orthoesters and Ketals: Application to the Synthesis of Furfuryl Ether Biofuels" *ACS Sustainable Chemistry & Engineering* **2018**, *6*, 4996–5002.
25. R. Wang, M. Zhang, Q. Wang, W. Zhang, H. Wang, M. Zheng, Z. Qu, Z. Zhou, P. Li, J.-H. Yang, "Silica gel supported Cu nanoparticles for selective reductive etherification of furfural into isopropyl furfuryl ether" *Journal of Alloys and Compounds* **2024**, *1008*, 176781.
26. N. Yamanaka, K. Nishi, K. Yasunaga, H. Yamada, "Synthesis of ethyl furfuryl ether via etherification of furfuryl alcohol with ethanol over montmorillonite K10" *RSC Advances* **2024**, *14*, 25221–25226.
27. N. L. Mulik, P. S. Niphadkar, V. V Bokade, "Synthesis of ethyl furfuryl ether (potential biofuel) by etherification of furfuryl alcohol with ethanol over heterogenized reusable $H_1Cs_2PW_{12}O_{40}$ catalyst" *Research on Chemical Intermediates* **2020**, *46*, 2309–2325.
28. J. Wang, X. Zhao, Q. Yang, X. Ren, X. Gong, X. Li, F. Wang, J. Jiang, H. Xu, Y. Guan, P. Wu, "Germanosilicates for selective etherification of biomass-derived furfuryl alcohol" *Applied Catalysis B: Environment and Energy* **2025**, *365*, 124956.
29. S. S. R. Gupta, M. L. Kantam, "Catalytic conversion of furfuryl alcohol or levulinic acid into alkyl levulinates using a sulfonic acid-functionalized hafnium-based MOF" *Catalysis Communication* **2019**, *124*, 62–66.
30. Y. Xu, X. Chen, C. Qiao, H. Wang, Y. Wang, Y. Tian, "Dynamics-driven tailoring of Zr-embedded hierarchical ZSM-5 zeolites for enhanced catalytic performance from furfural to alkyl levulinate" *Chemical Engineering Journal* **2024**, *486*, 150350.
31. R.-Q. Zou, H. Sakurai, S. Han, R.-Q. Zhong, Q. Xu, "Probing the Lewis Acid Sites and CO Catalytic Oxidation Activity of the Porous Metal–Organic Polymer [Cu(5-methylisophthalate)]" *Journal of the American Chemical Society* **2007**, *129*, 8402–8403.
32. K. L. Mulfort, J. T. Hupp, "Chemical Reduction of Metal–Organic Framework Materials as a Method to Enhance Gas Uptake and Binding" *Journal of the American Chemical Society* **2007**, *129*, 9604–9605.
33. B. Liu, H. Shioyama, T. Akita, Q. Xu, "Metal-Organic Framework as a Template for Porous Carbon Synthesis" *Journal of the American Chemical Society* **2008**, *130*, 5390–5391.
34. L. Chen, N. Tsumori, Q. Xu, "Quasi-MOF-immobilized metal nanoparticles for synergistic catalysis" *Science China Chemistry* **2020**, *63*, 1601–1607.
35. Y. He, Z. Yin, Z. Wang, H. Wang, W. Xiong, B. Song, H. Qin, P. Xu, G. Zeng, "Recent progress on mixed transition metal nanomaterials based on metal–organic frameworks for energy-related applications" *Journal of Materials Chemistry A* **2022**, *10*, 9788–9820.

36. S. Yi, W. Shi, X. Yang, Z. Yao, “Engineering sensitive gas sensor based on MOF-derived hollow metal-oxide semiconductor heterostructures” *Talanta* **2023**, *258*, 124442.
37. Q. Sun, H. Gao, M. Xiao, T. Sema, Z. Liang, “Cerium-MOF-Derived Composite Hierarchical Catalyst Enables Energy-Efficient and Green Amine Regeneration for CO_2 Capture” *Environmental Science & Technology* **2024**, *58*, 10052–10059.
38. Y. Zhang, R. Wang, **2025**, DOI: 10.3390/molecules30132836.
39. R. R. Salunkhe, Y. V Kaneti, Y. Yamauchi, “Metal–Organic Framework-Derived Nanoporous Metal Oxides toward Supercapacitor Applications: Progress and Prospects” *ACS Nano* **2017**, *11*, 5293–5308.
40. X. Dong, E. Yan, Y. Lv, Y. Zhou, X. Chu, “Engineering MOF-derived hollow metal oxides toward enhanced electrocatalytic oxygen evolution reaction” *Applied Catalysis A: General* **2024**, *681*, 119772.
41. L. Jin, B. Li, X. Qian, S. Zhao, H. Xu, “Synthesis of V_2O_3@C-CNTs nanocomposites via in situ growth of carbon nanotubes from V-MOF for enhanced lithium-sulfur battery separators” *Alloys and Compounds* **2025**, *1010*, 178108.
42. J. Kim, N. D. McNamara, J. C. Hicks, “Catalytic activity and stability of carbon supported V oxides and carbides synthesized via pyrolysis of MIL-47(V)” *Applied Catalysis A: General* **2016**, *517*, 141–150.
43. S. S. R. Gupta, M. L. Kantam, “Catalytic conversion of furfuryl alcohol or levulinic acid into alkyl levulinates using a sulfonic acid-functionalized hafnium-based MOF” *Catal. Commun.* **2019**, *124*, 62–66.
44. N. Mulik, V. Bokade, “Immobilization of HPW on UiO-66-NH2 MOF as efficient catalyst for synthesis of furfuryl ether and alkyl levulinate as biofuel” *Molecular Catalysis* **2022**, *531*, 112689.
45. U. S. F. Arrozi, I. Irnanda, M. R. Pratama, Y. Permana, S. H. Qurbayni, W. W. Lestari, W. Ciptonugroho, H. W. Wijaya, Y. P. Budiman, “Etherification of furfuryl alcohol catalyzed by vanadium-modified MOF-808: Thermocatalysis and UV-assisted thermocatalysis” *Appl. Catal. A Gen.* **2025**, *706*, 120472.
46. K. Barthelet, J. Marrot, G. Férey, D. Riou, “VIII(OH){O2C–C6H4–CO2}.(HO2C–C6H4–CO2H)x(DMF)y(H2O)z (or MIL-68), a new vanadocarboxylate with a large pore hybrid topology : reticular synthesis with infinite inorganic building blocks?” *Chemical Communications* **2004**, 520–521.
47. F. Carson, J. Su, A. E. Platero-Prats, W. Wan, Y. Yun, L. Samain, X. Zou, “Framework Isomerism in Vanadium Metal–Organic Frameworks: MIL-88B(V) and MIL-101(V)” *Crystal Growth & Design* **2013**, *13*, 5036–5044.
48. Y. Cai, G. Fang, J. Zhou, S. Liu, Z. Luo, A. Pan, G. Cao, S. Liang, “Metal-organic framework-derived porous shuttle-like vanadium oxides for sodium-ion battery application” *Nano Res.* **2018**, *11*, 449–463.
49. P. Hu, P. Hu, T. D. Vu, M. Li, S. Wang, Y. Ke, X. Zeng, L. Mai, Y. Long, “Vanadium Oxide: Phase Diagrams, Structures, Synthesis, and Applications” *Chem. Rev.* **2023**, *123*, 4353–4415.

50. K. Barthelet, J. Marrot, D. Riou, G. Ferey, “A Breathing Hybrid Organic - Inorganic Solid with Very Large Pores and High Magnetic Characteristics” *Angewandte Chemie International Edition* **2002**, *41*, 281–284.
51. Y. Zhang, M. Fan, X. Liu, C. Huang, H. Li, “Beltlike V2O3@C core-shell-structured composite: Design, preparation, characterization, phase transition, and improvement of electrochemical properties of V2O3” *Eur. J. Inorg. Chem.* **2012**, *2012*, 1650–1659.
52. K. Wu, Y. Wu, P. Fu, D. Yang, B. Ruan, M. Wu, R. Wu, “Composites of Vanadium (III) Oxide (V_2O_3) Incorporating with Amorphous C as Pt-Free Counter Electrodes for Low-Cost and High-Performance Dye-Sensitized Solar Cells” *ACS Omega* **2021**, *6*, 11183–11191.
53. X. Zhang, Z. Chen, X. Liu, S. L. Hanna, X. Wang, R. Taheri-Ledari, A. Maleki, P. Li, O. K. Farha, “A historical overview of the activation and porosity of metal–organic frameworks” *Chemical Society Reviews* **2020**, *49*, 7406–7427.
54. G. Wang, Z. Zhang, L. Song, “Efficient and selective alcoholysis of furfuryl alcohol to alkyl levulinates catalyzed by double SO3H-functionalized ionic liquids” *Green Chemistry* **2014**, *16*, 1436–1443.
55. Y. Yang, Q. Liu, Z. Liu, **2024**, DOI: 10.3390/catal14040223.
56. G. Di Carmine, C. Leonardi, L. Forster, M. Hu, D. Lee, C. M. A. Parlett, O. Bortolini, M. A. Isaacs, A. Massi, C. D’Agostino, “Humin Formation on SBA-15-pr-SO3H Catalysts during the Alcoholysis of Furfuryl Alcohol to Ethyl Levulinate: Effect of Pore Size on Catalyst Stability, Transport, and Adsorption” *ACS Appl. Mater. Interfaces* **2023**, *15*, 24528–24540.
57. Z. Liu, R. Zhang, H. Liu, J. Zhang, Y. Sun, N. Li, L. Peng, “Effect of carbon modifier on characteristics and catalytic properties of zeolite–carbon hybrid supported Zr towards γ-valerolactone production” *Fuel* **2024**, *359*, 130380.
58. S. E. Sih, F. Franco-Duro, C. García-Sancho, F. J. García-Mateos, J. M. Rosas, R. Moreno-Tost, P. Maireles-Torres, J. A. Cecilia, “Valorization of Furfural to Obtain High Value-Added Products with ZrO2- and Al2O3-Pillared Clays” *Top. Catal.* **2025**, *68*, 99–113.

Figures

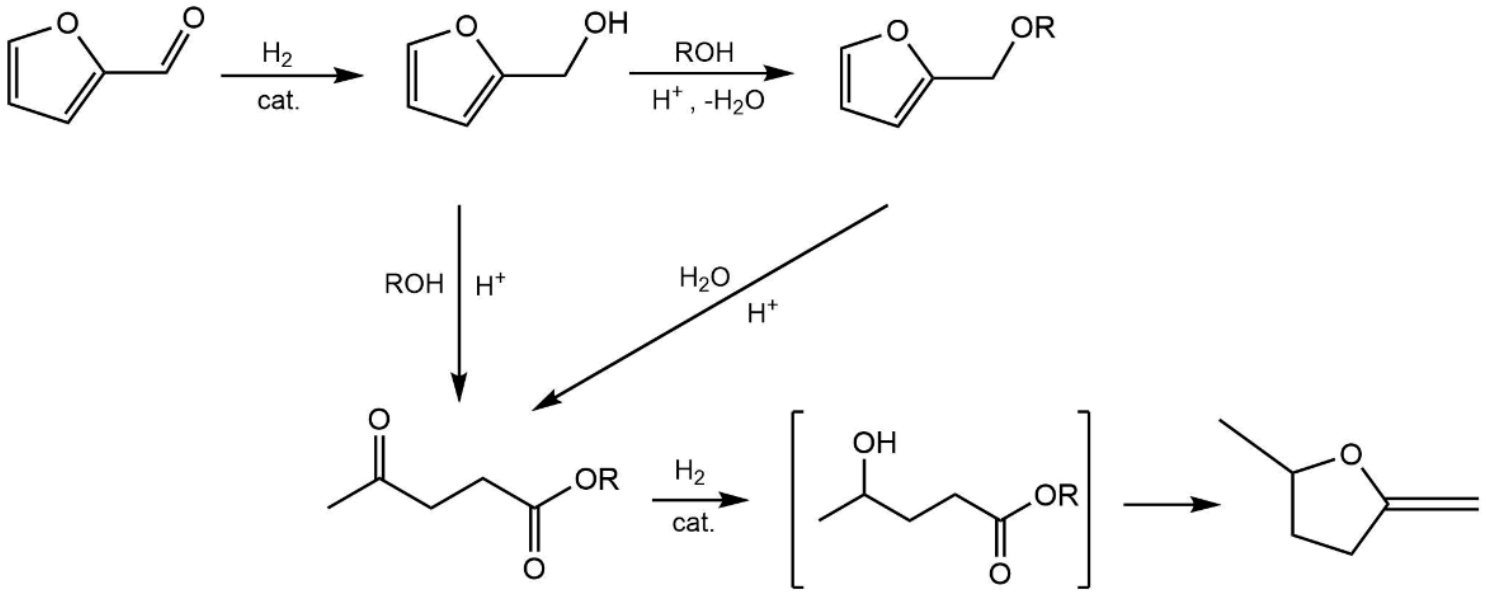


Figure 1

Schematic illustration of the reaction pathways converting furfural and furfuryl alcohol into alkyl furfuryl ethers and alkyl levulinates.

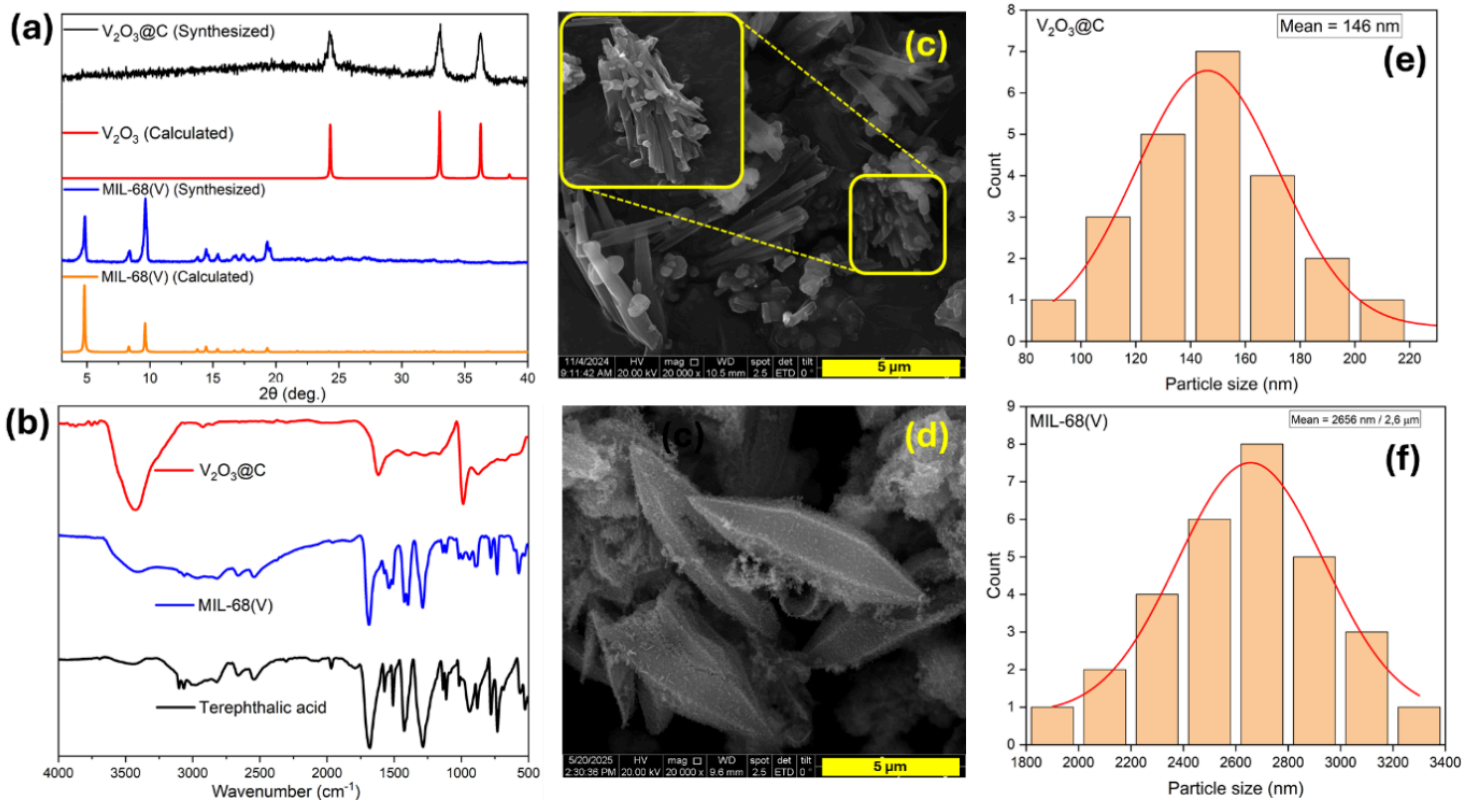


Figure 2

(a) PXRD patterns and (b) FTIR spectra of the MIL-68(V) and its oxide derivative, V_2O_3@C; SEM images of (c) MIL-68(V), (d) V_2O_3@C; Particle size distribution of (e) V_2O_3@C and (f) MIL-68(V).

Image not available with this version

Figure 3

Legend not included with this version.

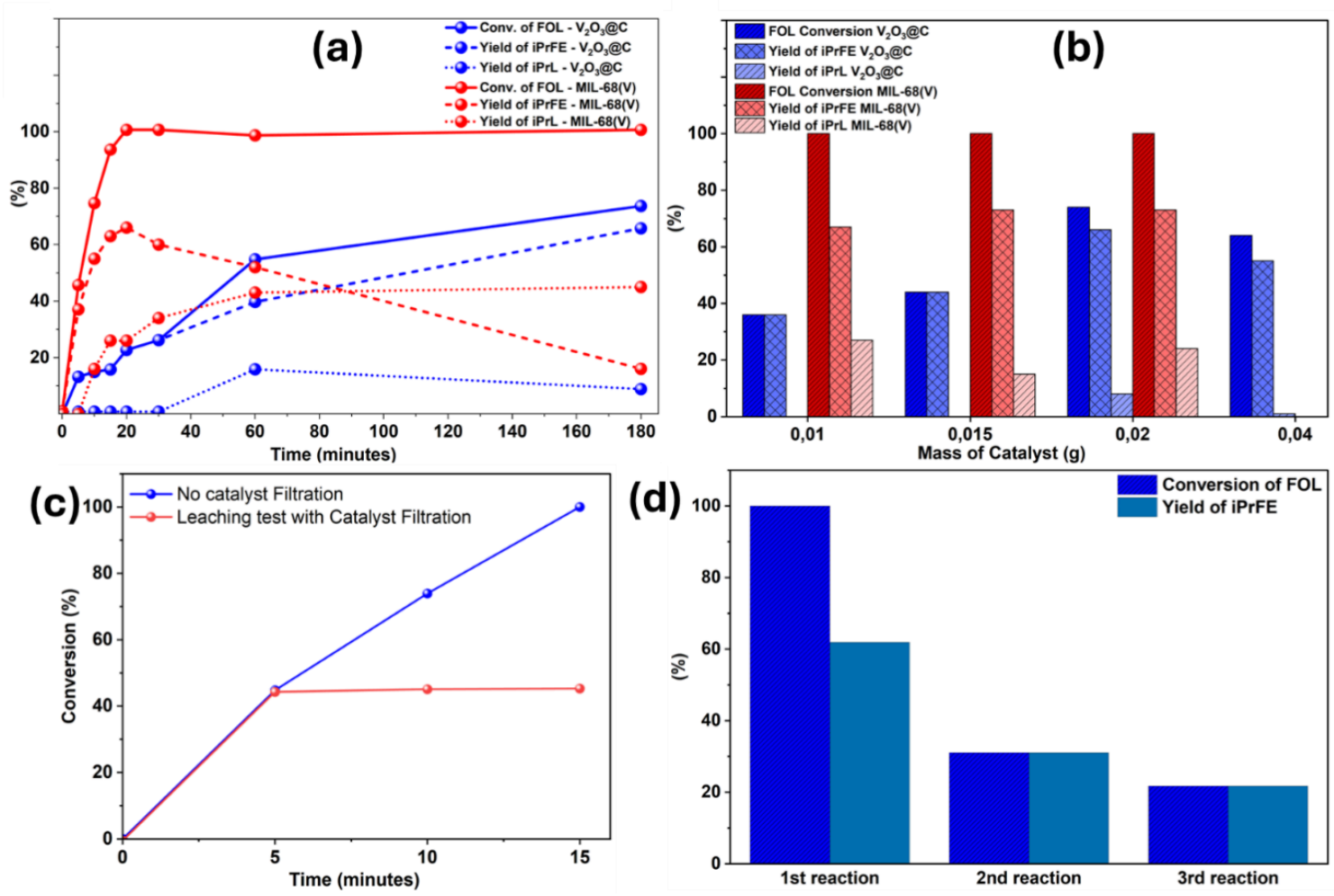


Figure 4

Etherification reaction of FOL with 2-propanol catalyzed by 0.016 mmol V_2O_3@C and MIL-68(V) under (a) different reaction time (reaction condition: catalyst = 0.02 g, 1.63 mmol FOL, 2.5 mL 2-propanol, T= 160 ℃), (b) different mass of catalyst (reaction condition with V_2O_3@C catalyst: 1.63 mmol FOL, 2.5 mL 2-

propanol, t = 180 min, T= 160 ℃; reaction condition with MIL-68(V) catalyst: 1.63 mmol FOL, 2 mL 2-propanol, t = 20 min, T= 160 ℃) (c) leaching test of MIL-68(V), and (d) reusability test of MIL-68(V) (reaction condition: 0.02 g of catalyst, 1.65 mmol FOL, 2.5 mL of 2-propanol, T= 160 ℃).

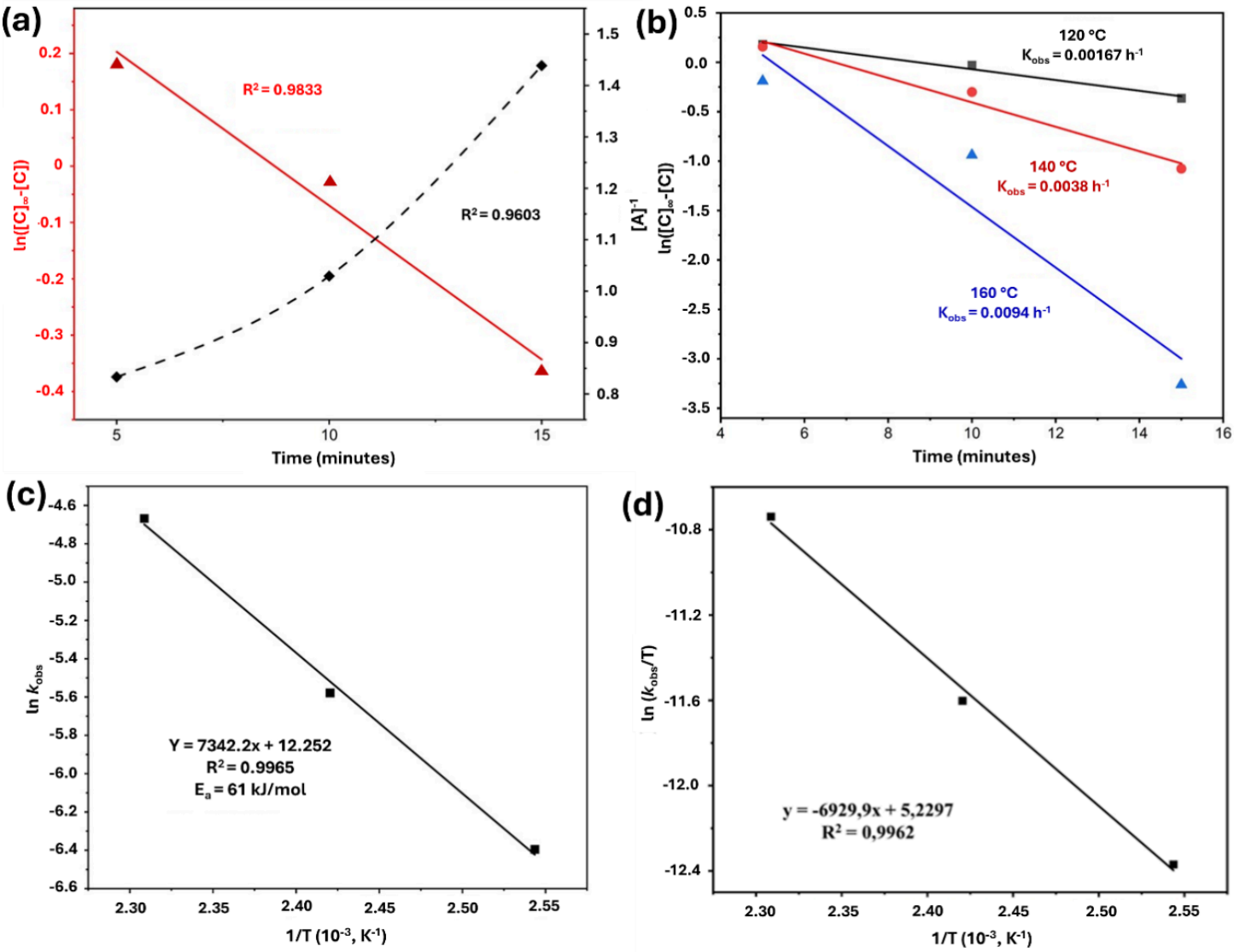


Figure 5

(a) Plots of ln$[C]_{\infty}$-[C] and 1/[FOL] versus reaction time (T= 160 °C); (b) A plot of ln $[C]_{\infty}$-[C] versus time at different reaction temperature; (c) A plot of ln k_{obs} vs 1/T; and (d) A plot of ln(k_{obs}/T) vs 1/T. [C] refers to [iPrFE].

Supplementary Files

This is a list of supplementary files associated with this preprint. Click to download.

- SIMIL68V2O3CEtherificationFOLEND.docx